Volume 1 | Number 1 | Jan 2013 | Pages 1–100

PCCP

Physical Chemistry Chemical Physics
www.rsc.org/pccp

ROYAL SOCIETY OF CHEMISTRY

ROYAL SOCIETY OF CHEMISTRY

www.rsc.org/pccp

Effect of Environment on Iodine Oxidation State and Reactivity with Aluminum

Dylan K. Smith[1], Jena McCollum[1], Michelle L. Pantoya[1*]

[1]Department of Mechanical Engineering, Texas Tech University, Lubbock, TX 79409
*Corresponding author contact information: Phone: 806-834-3733; email: michelle.pantoya@ttu.edu

Abstract

Iodine oxide is a highly reactive solid oxidizer and with its abundant generation of iodine gas during reaction, this oxidizer also shows great potential as a biocidal agent. A problem with using I_2O_5 in an energetic mixture is its highly variable reactive behavior. This study isolates the variable reactivity associated with I_2O_5 as a function of its chemical reaction in various environments. Specifically, aluminum fuel and iodine oxide powder are combined using a carrier fluid to aid intermixing. The carrier fluid is shown to significantly affect the oxidation state of iodine oxide, thereby affecting the reactivity of the mixture. Four carrier fluids were investigated ranging in polarity and water miscibility in increasing order from hexane < acetone < isopropanol < water as well as untreated, dry-mixed reactants. Oxidation state and reactivity were examined with experimental techniques including X-ray photoelectric spectroscopy (XPS) and differential scanning calorimetry (DSC). Results are compared with thermal equilibrium simulations. Flame speeds increased with polarity of the fluid used to intermix the powder and ranged from 180 to 1202 m/s. The I_2O_5 processed in the polar fluids formed hydrated states of iodine oxide: HIO_3 and HI_3O_8; and, the nonpolar and dry-mixed samples formed: I_2O_4 and I_4O_9. During combustion, the hydrated iodine oxides rapidly dehydrated from HIO_3 to HI_3O_8 and from HI_3O_8 to I_2O_5. Both steps release 25% of their mass as vapor during combustion. Increased gas generation enhances convective energy transport and accounts for the increase in reactivity seen in the mixtures processed in polar fluids. These results explain the chemical mechanisms underlying the variable reactivity of I_2O_5 that are a function of the oxide's highly reactive nature with its surrounding environment. These results will significantly impact the selection of carrier fluid in the synthesis approach for iodine containing reactive mixtures.

Key Words: iodine oxide, aluminum, combustion, reactivity, iodine pentoxide, iodic acid, polarity, hydration, oxidation state, pre-ignition reaction.

Introduction

Reactions between aluminum (Al) and iodine oxides have been studied extensively because they offer great potential for use as a biocidal agent in addition to generating energy [1–9]. Carrying iodine in the solid form (i.e., as an oxide compound) provides a means to easily transport iodine, then upon reaction, disperse gaseous iodine in a way that could neutralize air born bacteria [2,8,9]. In fact, incorporating iodine oxides into energetic materials is being considered as a way to neutralize the biological threat associated with weapons of mass destruction [8,9]. Aluminum is a high energy density fuel (i.e., heat of combustion equivalent to 30,372 J/g) that is often incorporated into explosives and other energetic material systems [10–13]. For this reason, research on aluminum and iodine oxide reactions not only provides an understanding of fundamental reactivity directly representative of an application, but also often includes an analysis of the response of bacteria to exposure from the reaction [2,8,9].

While Al particles have the potential to provide great calorific energy, much of the chemical energy stored in a single particle is rarely fully exploited. For many applications, aluminum combustion can be inefficient and incomplete [14,15]. A single spherical Al particle is actually a composite composed of an aluminum core encapsulated by an amorphous aluminum oxide shell [15,16]. The amorphous aluminum oxide shell can act as a barrier to the diffusion reaction between the aluminum fuel and a surrounding oxidizer [17]. However, on the nano-particle scale, the aluminum oxide layer has been shown to contribute exothermically to the overall energy liberated during certain types of reactions [18]. This observation escalated the shells role from barrier to exothermic participant in the reaction. Osborne and Pantoya first showed that when a fluoropolymer (i.e., polytetrafluoroethylene, PTFE) combines with nano-particle aluminum (nAl), a distinct exotherm exists prior to the main reaction of the core [18]. This

exothermic reaction is attributed to fluorination of the aluminum oxide shell to form aluminum fluoride (AlF_3) and has been coined the pre-ignition reaction (PIR) [18]. Later work showed that manipulating the PIR kinetics can influence the overall reactivity of the mixture. This was an insightful contribution to our understanding of nAl combustion because it offered a new strategy for optimizing reactivity: by activating a PIR with the alumina shell that effectively catalyzes combustion.   For this reason, a new direction for research has been to modify the structure of the outer aluminum oxide shell to enhance early stage reaction kinetics (i.e., the PIR).

One study modified the aluminum oxide structure simply by varying the polarity of the carrier fluid used to intermix aluminum with a fluoropolymer oxidizer [19]. Specifically, Padhye et al. studied the influence of different fluids varied by polarity used to mix powders. The carrier fluid used to process mixtures showed a significant influence on the reactivity of the dried powder mixture [19]. They showed that for Al with PTFE, PIR reactivity is a function of -OH bonding and the concentration and accessibility of the hydration layer increases for powder processing in polar fluids. The hydroxyl growth on the aluminum oxide shell increased the PIR and overall reactivity of the mixture. Interestingly, other halogens, including iodine, have been shown to exhibit a similar PIR behavior. For this reason, we predicted that fluid polarity may similarly enhance PIR reaction kinetics for Al and iodine oxide mixtures and lead to greater overall reactivity.

In preliminary work, we isolated fluid treatment to just the iodine oxide and found that I_2O_5 is far more affected by fluid polarity than Al. Iodine pentoxide (I_2O_5) is hygroscopic to the point of being deliquescent[20]. This property allows I_2O_5 to change its oxidation state readily in a humid environment. Equation (1) shows the hydration steps of I_2O_5 when exposed to water[4].

$$Hydration: 3I_2O_5 + 3H_2O \rightarrow 2HI_3O_8 + 2H_2O \rightarrow 6HIO_3 \tag{1a}$$

$$Dehydration: 6HIO_3 \rightarrow 2HI_3O_8 + 2H_2O \rightarrow 3I_2O_5 + 3H_2O \tag{1b}$$
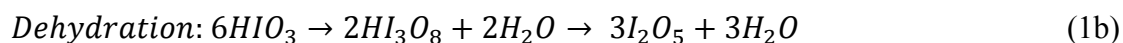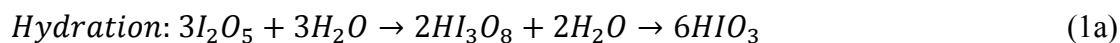
Little et al. [4] found that after being dissolved and recrystallized, I_2O_5 samples that were exposed to a relative humidity level of below 2% recrystallized back into I_2O_5. When exposed to less than 50 % relative humidity, I_2O_5 readily formed HI_3O_8; and, above 70% relative humidity, I_2O_5 was almost completely recrystallized into HIO_3[4,20]. This process is reversed with the addition of heat. At 110°C HIO_3 dissociates into HI_3O_8 and H_2O; and, at 210°C HI_3O_8 forms I_2O_5 and H_2O.

These findings have important implications for the fluid selected to intermix energetic composites that include iodine oxide. The objective of this project is to understand how fluid polarity influences the structure and state of iodine oxide and the resulting reactivity of the aluminum and iodine oxide mixture. This objective is accomplished through flame propagation measurements from mixtures processed using various fluids ranging from non-polar to polar (i.e., in order of increasing polarity: hexane < acetone < isopropanol < water) as well as dry mixing reactants. Additional characterization includes differential scanning calorimetry (DSC), thermal gravimetric analysis (TGA) and x-ray photoelectronic spectrometry (XPS). Thermal equilibrium simulations were also performed to help quantify variations in combustion properties such as gas generation and flame temperature.

Experimental

Reagents. Aluminum particles with an average diameter of 80nm were supplied by NovaCentrix (Austin, TX) and used as the fuel. These particles are passivated with an aluminum oxide shell between 2-3nm thick which allows them to be handled in a laboratory atmosphere. Diiodine pentoxide (I_2O_5) supplied by Aldrich (St. Louis, MO) was used as an oxidizer. These particles came in large crystals and were ground into a powder using a mortar and pestle. Three hydrocarbon fluids were used, hexane (Fisher), isopropanol (Macron Fine Chemicals) and acetone (Macron Fine Chemicals) all of which are reagent grade or better and used without further purification. The water content of each of the hydrocarbon fluids was determined by volumetric titration and found to be 0.9 vol. % and 0.1 vol.% for acetone and isopropanol respectively and negligible for hexane [21]. Water was also used as a carrier fluid. This water was normal tap water run through a Millipore Millipak® 100 filter with a 0.22μm pore size.

Sample Preparation. All samples were prepared using an equivalence ratio of 1.0 for Al fuel and I_2O_5 oxidizer. To ensure good dispersion, each sample was suspended in 60 ml of each of the fluids and sonicated at 3W for a total of 60 seconds in 10 second on/off intervals. The samples were then poured into a Pyrex dish and placed in a fume hood at room temperature and allowed to dry. The powders were reclaimed and sieved after a minimum of 24 hours in the fume hood.

Reaction Kinetics. A flame tube apparatus know as a Bockmon Tube was used to measure flame speeds. The quartz tubes are 7 cm long with a 3 mm inside diameter and filled to a consistent bulk density of $18 \pm 2\%$ of the theoretical maximum density (TMD) for the Al + I_2O_5 mixture. The quartz tube was placed inside a combustion chamber with viewing port and a

high speed camera was aligned perpendicular to the direction of flame propagation. Imaging was performed using a Phantom v1611 high-speed camera (Vision Research Inc.) at 381,818 fps at a resolution of 384 x 64 pixels. The Phantom Camera Control (PCC) program was used to track and record flame front propagation. The time and distance measurements were exported into spreadsheet software where they were plotted and fit to a linear curve. All data reported produced an R^2 value greater than 0.95.

Thermal Equilibrium Analysis. Thermal analysis was performed using a Netzsch model STA 449 differential scanning calorimeter/ thermal gravimetric analyzer (DSC/TGA). Samples were prepared by sonication of Al, I_2O_5, or powder mixtures processed in a fluid then allowed to dry in a similar manner as the flame speed samples. The dry-mixed and fluid processed $Al+I_2O_5$ samples were heated to 1000 °C at 10 °C/min. The dry-mixed and fluid treated I_2O_5 samples were heated to 350 °C at 10 °C/min to examine the pre-ignition reactions (PIR) more closely. All samples were analyzed in an argon environment and experiments were performed in triplicate to ensure repeatability.

X-ray Photoelectron Spectroscopy (XPS). X-ray photoelectron spectroscopy was performed on the untreated (i.e., dry-mixed), hexane, and acetone samples before combustion using a PHI 5000 Versa Probe with an Al Kα source. Samples were loaded into a vacuum chamber and held to 1×10^{-6} Torr and 27 °C for 48 hour prior to and during measurement. Peaks were referenced to a C1s value of 284.8 eV for evaluation.

Thermal Equilibrium Simulations. Heats of combustion and gas generation were calculated using thermal equilibrium software, REAL code, and based on the formation enthalpy and mass fraction of the reactants. These simulations were performed assuming a constant

volume of 0.01 m³/kg, temperature of 2000°C, and internal energy equal to zero. For each

simulation, a stoichiometric mixture of Al, Al$_2$O$_3$ and I$_2$O$_5$ was assumed. This calculation also

assumes complete combustion (i.e., all Al is converted to Al$_2$O$_3$). Heat of formation for each

compound was determined assuming the elemental forms of the constituents form the products

(i.e., I$_2$ + 2.5O$_2$ →I$_2$O$_5$).

Results

Figure 1 shows the reactivity of each sample represented in terms of flame speed. The

untreated (dry mixed) sample produced a flame speed of 180 m/s. Samples treated in hexane,

acetone, isopropanol, and water exhibited flames speeds of 340, 801, 935 and 1202 m/s,

respectively. The fluid used to intermix reactants clearly influences energy propagation. The

dramatic differences shown in Fig. 1 have implications for the use of these materials in enclosed

or semi-enclosed systems.
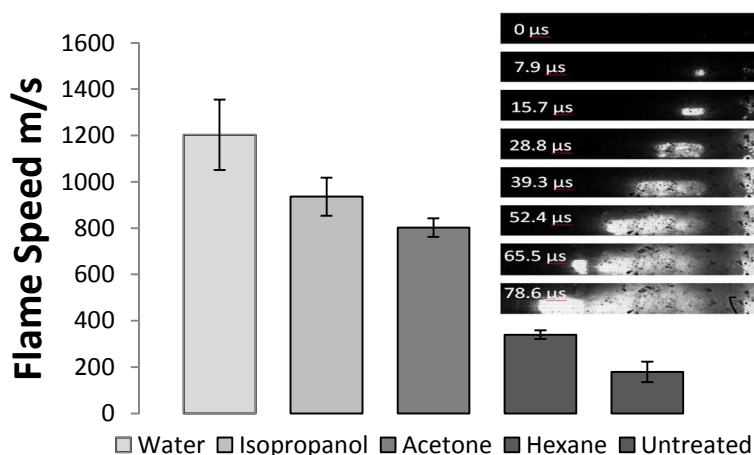
Figure 1. Flames speeds of nAl + I$_2$O$_5$ intermixed as a dry-mixture or processed with a carrier fluid such as hexane, acetone, isopropanol, and water that is evaporated prior to flame speed experiments. The inset shows still frame images of flame propagation in the tube that are time stamped. The representative sequence of images is for Al+I$_2$O$_5$ processed in isopropanol.

The heat flow trends from the DSC results for I_2O_5 (i.e., no Al) treated in the different fluids are shown in Fig. 2. Although carrier fluid evaporated from each sample prior to analysis, all fluid treated powders produce endotherms between 70 and 150 °C. The untreated, hexane and water treated samples have two peaks at the first endotherm while acetone and isopropanol treatments have only one. All of the treatments produced a single endotherm between 200 and 250 °C. The onset temperature for all endotherms and energy associated with the endothermic reaction (i.e., area under the curve) are shown in Table 1.

A.

B.
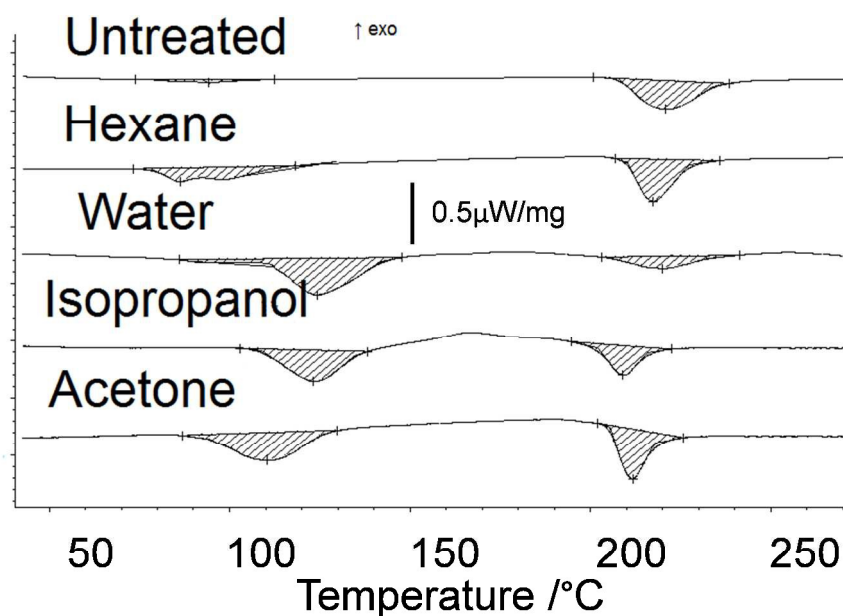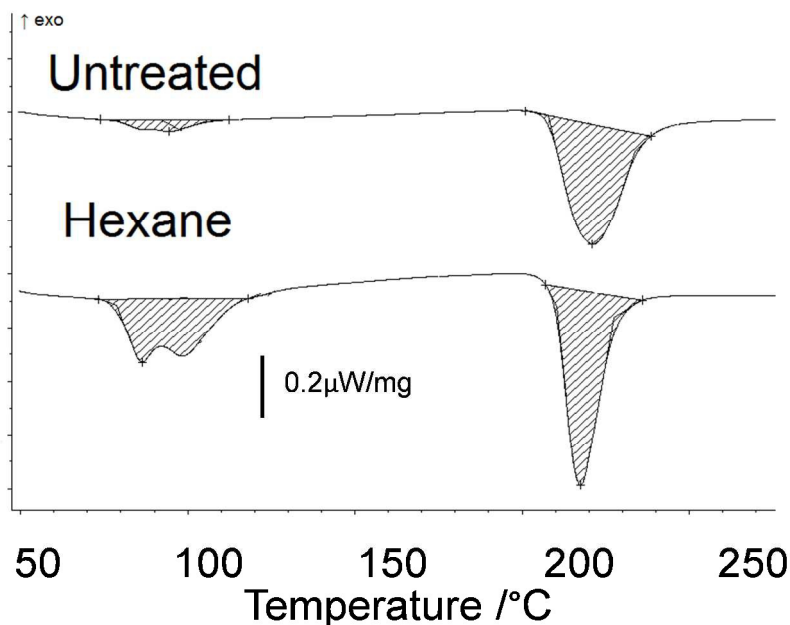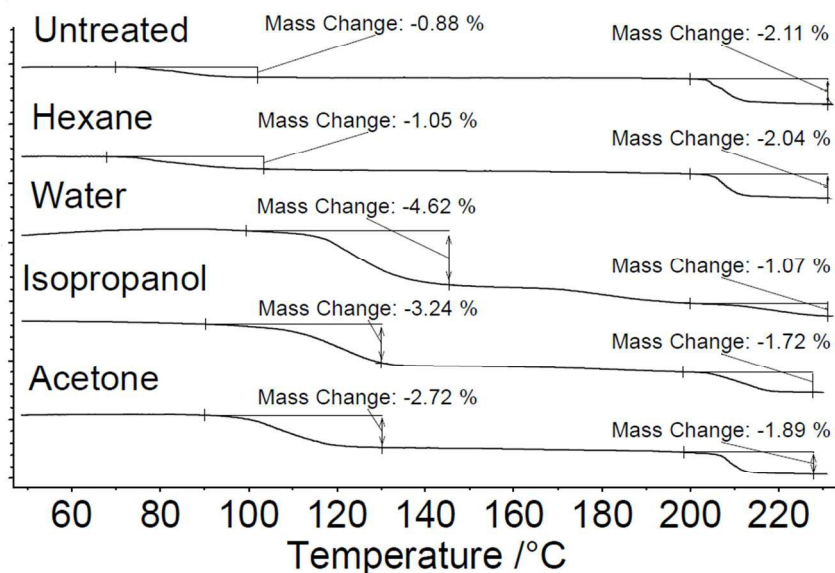
C.

Figure 2. A. Heat flow curves of I_2O_5 untreated and treated in hexane, isopropanol, acetone, and water. Fluids were evaporated prior to analysis. Samples were analyzed in an argon environment to 350 °C at 10 °C/min; and, B enlarged hexane and untreated heat flow curves, presented to clearly show two peaks associated with the first endotherm. C. Corresponding mass loss curves for the TG analysis.

Table 1. Summary of onset temperature and energy (i.e., total area under the curve) for heat flow curves shown in Fig. 2. All temperatures are reported in °C, energy is J/g, and mass loss is percent of total mass.

Treatment	1st Endotherm				2nd Endotherm		
	1st Onset Temp	2nd Onset Temp	Specific Energy	Mass Loss	Onset Temp	Specific Energy	Mass Loss
Untreated	79.4	87.3	4.6	0.88	207.8	48.9	2.11
Hexane	78.9	90.9	35.6	1.05	209.6	50.4	2.04
Isopropanol	107.8	-	67.6	3.24	203.4	40.5	1.72
Acetone	101.5	-	61.46	2.72	211.5	44.7	1.89
Water	96.8	115.1	78.48	4.62	205.9	19.9	1.07

The heat flow behavior from DSC measurements for $Al + I_2O_5$ are shown in Fig. 3. The mixtures show the same endotherms between 75 and 125 °C and between 200 and 250 °C that are seen in the I_2O_5 sample (see Fig. 2 and Table 1). Also, there are exotherms between 350 and 450 °C and between 450 and 600 °C for all samples. The onset temperature, energy (area under the curve), and mass loss for all the exotherms are summarized in Table 2.
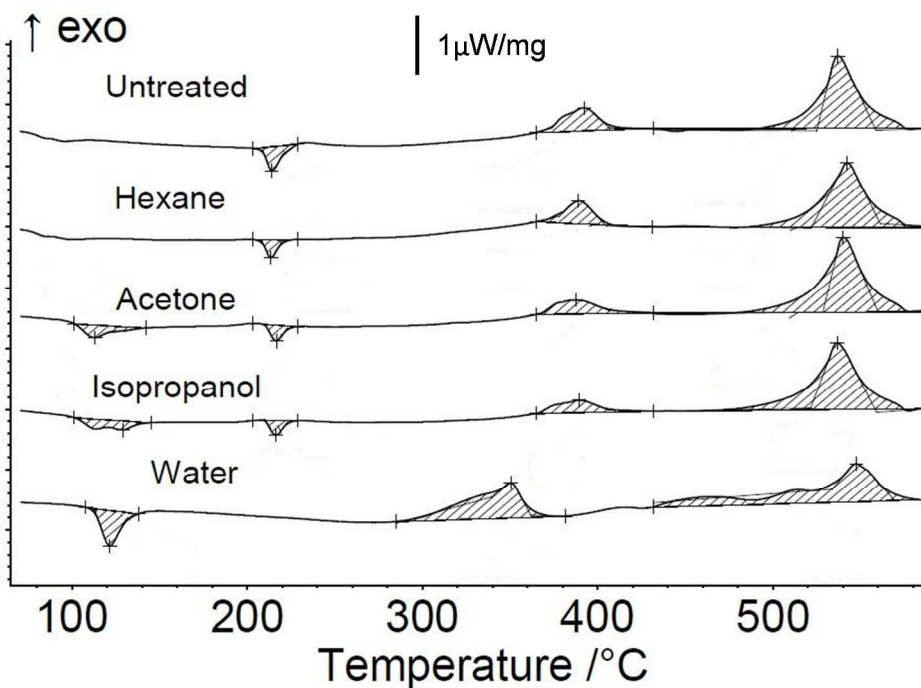
Figure 3. Heat flow curves of Al-I$_2$O$_5$ samples untreated and treated in hexane, acetone isopropanol, and water. Samples were run in an argon environment to 700 ^{o}C at 10 ^{o}C/min.

Table 2. Summary of temperature and energy data from Fig. 3. Note PIR is pre-ignition reaction and all temperatures are in °C and specific energy is J/g.

Treatment	PIR		Main Reaction	
	Onset Temperature	Specific Energy	Onset Temperature	Specific Energy
Untreated	372.8	71.4	521.6	305.4
Hexane	378.4	61.6	519.4	290.0
Acetone	367.5	64.0	522.6	323.3
Isopropanol	367.3	58.2	521.5	314.7
Water	287.6	182.9	435.9	265.8

X-ray photoelectron spectroscopy (XPS) general survey and tight scans for the 3d peak are shown for acetone in Fig. 4. Results for the untreated and hexane treated samples can be found in Fig. S1 and S2 (supplemental information).
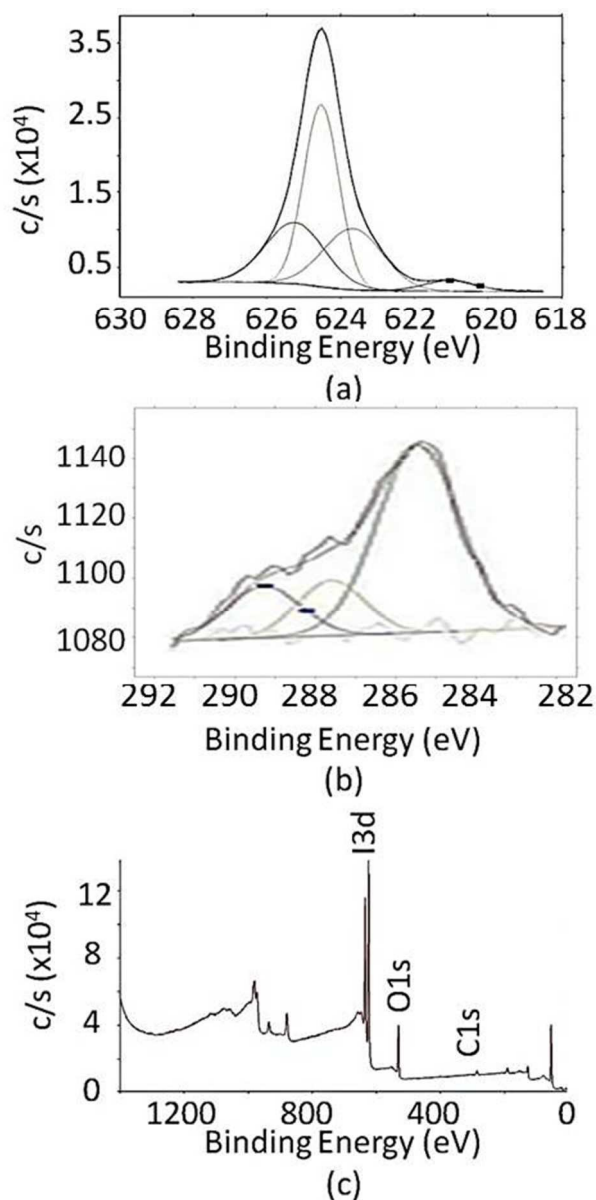
Figure 4. XPS spectra for acetone-treated I_2O_5 samples where (a) is the tight scan iodine $3d_{5/2}$ peak, (b) is the tight scan C1s peak and (c) is the survey scan for all binding energies.

Binding energies (BE) were compared to peaks identified by Sherwood[22] for I_2O_5, HIO_3, HI_3O_8 and I_2 which are listed in Table 3. Binding energies and percentage of the compound for our deconvoluted spectra are shown in Table 4. The amount of carbon in each sample relative to the untreated sample is shown in Table 5. The carbon seen in this analysis is adventitious carbon.

The C-O and C=O peaks represent the adventitious carbon binding to the oxygen species in the sample. The oxygen end of the C-O and C=O bonds could come from the other oxygen containing species (i.e., I_2O_5, HIO_3, etc.).

Table 3. Iodine $3d_{\frac{5}{2}}$ electron peaks from Sherwood[22].

Oxidation state	Binding Energy(eV)
I_2	619.9
HIO_3	623.1
HI_3O_8	623.2
I_2O_5	623.3

Table 4. Binding energy values for the deconvoluted $I3d_{5/2}$ spectra.

Sample	I_2		HIO_3		HI_3O_8		I_2O_5	
	BE	% I_2	BE	%HIO_3	BE	%HI_3O_8	BE	%I_2O_5
Untreated	621.0	4	624.4	13	624.5	53	624.6	30
Hexane	619.9	3	623.1	22	623.2	42	623.3	33
Acetone	619.3	4	623.0	25	623.8	45	624.5	26

Table 5. Binding energy (BE) values for the deconvoluted C1s spectra.

Sample	C-C BE	C-O BE	C=O BE
Untreated	284.8	286.3	288.3
Hexane	284.8	286.8	288.7
Acetone	284.8	286.9	288.5

Results indicate that all three samples contain approximately the same concentration of I_2. There is less HIO_3 in the untreated and hexane samples than there is the acetone sample. There is more HI_3O_8 in the untreated samples than there is in the hexane and acetone treated samples. There is very little difference in the amount of I_2O_5 between samples. Acetone showed a much greater carbon profile than the untreated and hexane treated samples.

Thermal Equilibrium Simulation

Tables 6 shows heat of formation for I_2O_5 and HIO_3 and heat of combustion when reacted with a stoichiometric mixture of Al. Table 7 shows the gas generation of Al + I_2O_5 and the gas generation of the dehydration steps. The dehydration of the iodic acids, both of which absorb heat, release 25% of their products in vapor phase.

Table 6. Heat of formation and heat of combustion for stoichiometric mixture for the different iodine oxidation states and aluminum

Molecule	ΔH_f (kJ/kg)	Heat of combustion (kJ/kg)
I_2O_5	-526.4	5850
HIO_3	-1308.1	5583

Table 7. Gas generation for aluminum and iodine combustion and for the dehydration of iodine oxidation states at 2000°C.

Reaction	% gas
$10\,Al + 3I_2O_5 \rightarrow 5Al_2O_3 + 6I_2$	75%
$2HI_3O_8 Dehydration$	25%
$3HIO_3 \rightarrow Dehydration$	28%

Discussion

The flame speed results can be separated into two sets according to high and low speeds: the higher speeds correspond to samples processed in polar fluids and lower speeds correspond to the samples processed in non-polar fluid (hexane) or the untreated (dry-mixed) samples. The difference between the hexane and untreated samples is significant, but generally five times smaller than the difference between the average speeds of the samples processed in polar fluids. The flame speed difference between the hexane treated and untreated samples can be attributed to inhomogeneity in the untreated samples, which limits proper dispersion of the reactants. For this reason, nearly every mixing approach involves a carrier fluid to improve dispersion quality. Employing hexane allows for a more homogeneous mixture, which improves reaction efficiency resulting in more complete combustion and higher flame speeds. In addition to dispersion quality, samples treated in polar fluids show improved reactivity.

For all samples, Fig. 2A shows endotherms at 210 °C that correlate to dehydration of HI_3O_8 [4]. This is consistent with findings by Kumar et al. [20], because the relative humidity never dropped below 2% so the natural deliquescent properties of I_2O_5 caused recrystallization partially into HI_3O_8. This finding is confirmed by XPS results (see Fig. 4 and S1 and S2) that show all samples consist of > 40% HI_3O_8. Figure 2 shows the first endotherm occurs at 110 °C for acetone, isopropanol, and water treated samples. This first endotherm correlates to the temperature HIO_3 dissociates into HI_3O_8 and H_2O and indicates that these samples are at least partially composed of HIO_3. This change in oxidation state is attributed to water concentration in the carrier fluids and atmospheric water. One gram of powder is sonicated in 60 ml of carrier fluid such that enough water is available to recrystallize a portion of I_2O_5 into HIO_3.

Concentration of iodic acid can be calculated in a method shown in Selte et al.[23] using the hydration and dehydration mechanism in Eq. (1). Using this method, mass loss at 110°C and 210°C will be 5% if the sample is completely composed of iodic acids. This method accurately describes iodic acid dehydration when heated slowly from ambient temperature to the reaction temperature and correlates well with our results for all samples other than the water treated samples, which all had total mass losses under 5%. The water treated samples had mass losses above 5% suggesting liquid water was still present that did not chemically react with I_2O_5 to form HIO_3.

During combustion, there is rapid dehydration of HIO_3 and HI_3O_8. In both steps of the reaction shown in Eq. (1b), thermal chemical equilibrium calculations show that 25% of the products are water vapor, iodine, and oxygen (Table 7). The TGA mass loss results differ from thermal equilibrium calculations because the calculations assume a temperature of 2000°C, which more accurately represents conditions of dehydration during combustion. Gas release causes the reaction to be more convectively dominant thereby increasing flame speeds, especially in tube confinement. In the reaction of I_2O_5 and Al, intermolecular bonds holding I_2O_5 together must be broken before Al can react with the oxygen from the I_2O_5. This reaction happens at 400°C. When I_2O_5 is combined with water, HIO_3 is formed which dehydrates at 110°C. Under thermal equilibrium conditions, the products of the dehydrated HIO_3 recombine to form I_2O_5. During ignition, the products of HIO_3 dehydration do not have time to recombine to form I_2O_5. Energy that would be needed to break intermolecular I_2O_5 bonds at 400°C are replaced with hydrogen bonds that are broken at 110°C. The polarity of water provides the energy needed to chemically transform I_2O_5 into HIO_3 and allows intermolecular I_2O_5 bonds to be broken at a lower temperature. This difference in energy allows for the convective influence

of the gas produced to increase flame speeds. Because of this, addition of more water than is

needed to chemically transform I_2O_5 into HIO_3 will slow flame speeds.

Another contribution to gas generation may be from Al reaction with water to produce

hydrogen gas[24–27]. While studies have shown hydrogen gas production rates are slow at room

temperature (i.e., an induction time of 15 hours), at elevated temperatures increased hydrogen

gas production becomes more dominant. In this way, the polar fluids may also enhance

convective energy transport by an additional contribution of hydrogen gas production from

residue water reacting with aluminum. However this gas generation rate is anticipated to be less

dominant than gas generated from the iodic acids.

The fluids also induce a change in oxidation state of I_2O_5. In the untreated and hexane

treated samples, the first endotherm has peaks that correspond to melting points of iodine

tetroxide (I_2O_4) and iodine nonaoxide (I_4O_9)[28]. To the authors' knowledge, this endothermic

activity has never been recorded. Ditte's reaction[21] is shown in Eq. 2 and for temperatures above

65 °C, I_2O_5 oxidizes carbon monoxide into carbon dioxide readily. This process is slowed below

65 °C and can account for the small endothermic peaks corresponding to I_2O_4 and I_4O_9 in the

untreated samples (see Fig. 2)

$$5CO + \ I_2O_5 \ \rightarrow 5CO_2 + I_2 \qquad\qquad\qquad \text{Eq (2)}$$

The intermediate steps involved with carbon containing compounds, atmospheric oxygen and

iodine can form I_2O_4, I_4O_9 [23]. However, Wikjord et al.[29] showed an exothermic reaction at 180°C

when I_4O_9 thermally decomposes into I_2O_5 which is not seen with our samples. A combination of

hydration and chemical reaction with carbon could account for endothermic activity seen below

100°C in the untreated and hexane treated samples. A more in depth study is needed to understand this reaction.

The XPS results shown in Fig. 4 support the claim that oxidation of carbon has a significant influence on overall reactivity. Carbon peaks in XPS data are usually significantly greater than carbon peaks found in these samples. Here samples were held under vacuum for 24 hours which eliminates all water and carbon monoxide from the chamber. The lack of water and carbon monoxide allows the carbon in the sample to react with I_2O_5 similar to Eq. 2. Carbon reacts with oxygen from I_2O_5 and forms gas phase carbon dioxide which is removed by the vacuum pumps. If this process occurs, we would expect to see I_2O_4 or I_4O_9 in the XPS results, but I_2O_4 and I_4O_9 are less stable than I_2O_5 and the iodic acids and could dissociates under vacuum. Another possible reason for not seeing I_2O_4 and I_4O_9 in the XPS results is the resolution and deconvolution of the XPS spectra. The difference in binding energies is 0.1 eV between the different oxidation states of the iodine oxides. The very close binding energies leave more combinations of possible deoconvolutions. With six peaks instead of four, there are exponentially more combinations that could result in the observed XPS spectra. This is one reason why there is very little literature available about the binding energies of I_2O_4 and I_4O_9. The lack of advantageous carbon is further evidence that the oxidation of carbon by I_2O_5 results in the lower oxidation states of I_2O_4 and I_4O_9 in the absence of water.

The endothermic peaks for I_2O_4 and I_4O_9 are greater for the sample processed in hexane than the untreated sample. It has been shown that water, due to its high hydration power, diminishes the oxidizing activity of inorganic(and organic) oxidants[30]. When not exposed to water, I_2O_5 readily oxidizes other compounds. Hexane has no water immiscibility, so the only water available during recrystallization comes from the humidity in the atmosphere and is

accounted for in the endothermic peak that correlates to the decomposition of HI_3O_8 into I_2O_5 and H_2O. Because of this, it is assumed that in the absence of water, I_2O_5 oxidizes hexane and carbon monoxide at an increased rate leaving behind I_2O_4 and I_4O_9 which accounts for the larger endothermic peaks at the melting points of I_2O_4 and I_4O_9 in the hexane treated sample compared to the untreated sample.

The lower oxidation states of I_2O_4 and I_4O_9 leave less oxygen available to react with Al during combustion. The combination of having I_2O_5 oxidation states with less readily available oxygen and the smaller influence from rapid dehydration (see Eq. (1b)) to form less water vapor account for the significant difference in flame speed between samples processed in polar fluids and samples processed in hexane or the dry-mixed case.

Oxidation of Alcohol

Oxidation of the fluids has another effect on flame speed. We have shown that water vapor increases flame speed for this mixture reacting under the confined conditions in the tube. But we have also shown that there is more water in acetone (0.9%) than in isopropanol (0.1%). This suggests that isopropanol should have a slower flame speed than acetone, which is in contradiction to our observations (see Fig. 1). This can be explained by the oxidation of alcohol with I_2O_5 which is described by Eq. (3)[6].

$$I_2O_5 + 10ROH \rightarrow I_2 + 10RO + 5H_2O \qquad\qquad \text{Eq. (3)}$$

The reaction from Eq. (3) releases water which may then hydrate the remaining I_2O_5 and could account for the increased flame speed for isopropanol processed samples compared with acetone. Clearly, I_2O_5 readily reacts with the environment and the fluids used for intermixing. The reactions that release oxygen from I_2O_5 also alter the stoichiometry of the mixture. Normally a

slightly fuel rich mixture increases flame speeds. A lean mixture could increase flame speeds because ancillary reactions between I_2O_5 and the environment during mixing that are not considered when determining stoichiometry could create an inadvertently fuel rich mixture.

Pre Ignition Reaction (PIR)

The PIR is an exothermic reaction that happens between the oxidizer and the alumina shell of the aluminum particles before the onset of the reaction between the aluminum core and oxidizer. This reaction has been shown to occur with fluorine and iodine[31]. It has also been shown that because of increased specific surface area of nAl particles, the PIR is greater with nAl than its micron scale counterpart [1]. In the $Al + I_2O_5$ reaction, I_2O_5 dissociates into I_2 , O_2 and IO fragments that can react with the Al_2O_3 passivation shell to form I-O-Al bridge bonds[31]. The dissociation of I_2O_5 is endothermic and has been studied extensively[1,31]. In Fig. 3, there is an exotherm that starts before 390 °C for the $Al + I_2O_5$ samples processed in all the fluids. The change from endotherm to exotherm at the I_2O_5 dissociation temperature indicates that IO fragments may be reacting with the alumina shell and exhibiting a PIR. Table 2 shows the onset temperature and specific energy of $Al + I_2O_5$ mixed in each carrier fluid as shown in Fig. 3. There is no significant difference between the onset temperature and specific energy of the hexane treated sample and the acetone and isopropanol treated samples. This shows us that the polarity of the carrier fluid does not induce a noticeable change in the PIR. However, there is significant difference in the PIR and main reaction between the water treated samples and all the other samples. Both the onset temperature and specific energy are reduced by 15% for the main reaction. For the PIR, the onset temperature is reduced by 23% and the specific energy is increased by 285% in the water treated sample when compared to the averages of the other samples. Figure 3 shows no endotherm at 210°C for the water treated sample indicating there is

no HI_3O_8 in the sample. Unlike fluorination of the aluminum oxide shell that is significantly affected by the polarity of the fluid used to process powders, iodination of the aluminum oxide shell is not affected by polarity of the fluid. Instead, the fluid significantly affects the hydration state of iodine oxide thereby influencing reactivity by purposefully introducing a gas generating agent that enhances convective energy transport.

Conclusions

Aluminum and iodine oxide $(Al + I_2O_5)$ powder mixtures, like most thermites, are processed using a carrier fluid to aid intermixing. This study showed that the carrier fluid significantly impacts the reactivity of the mixture and specifically effects the oxidation state of I_2O_5. Iodine oxide is hygroscopic to the point of being deliquescent. This property makes the oxidation state of iodine oxide highly dependent on water immiscibility in the carrier fluid. The different fluids used were shown to create five different oxidation states, I_2O_5, I_4O_9, I_2O_4, HIO_3 and HI_3O_8. The non-polar fluid and the untreated (i.e., dry) mixture contained negligible water. Because water reduces the oxidation ability of I_2O_5, the lack of water allows I_2O_5 to react (i.e., give up oxygen) with the fluid and even carbon monoxide in the atmosphere. These reactions leave lower oxidation states of iodine oxide (I_2O_4 and I_4O_9) which, when reacted with aluminum, have less available oxygen and generate less gas.

The polar fluids allow water to react with I_2O_5 and produce iodic acid (i.e., HIO_3 and HI_3O_8). When ignited, these oxidation states of iodic acid rapidly dehydrate. In this dehydration, 25% of the final mass is in a gas or vapor phase. The large amount of gas generation causes the reaction to be convectively driven and accounts for the increase in flame speed, especially in

confinement. Water inhibits the reduction of I_2O_5 during processing in the fluids and increases the amount of gas generation during reaction, both increase energy transport during reaction.

Acknowledgements

References

(1)   Farley, C.; Pantoya, M. Reaction Kinetics of Nanometric Aluminum and Iodine Pentoxide. *J. Therm. Anal. Calorim.* **2010**, *102* (2), 609–613.

(2)   Clark, B. R.; Pantoya, M. L. The Aluminium and Iodine Pentoxide Reaction for the Destruction of Spore Forming Bacteria. *Phys. Chem. Chem. Phys.* **2010**, *12* (39), 12653–12657.

(3)   Zhang, S.; Schoenitz, M.; Dreizin, E. L. Iodine Release, Oxidation, and Ignition of Mechanically Alloyed Al-I Composites. *J. Phys. Chem. C* **2010**, *114* (46), 19653–19659.

(4)   Little, B. K.; Emery, S. B.; Nittinger, J. C.; Fantasia, R. C.; Lindsay, C. M. Physiochemical Characterization of Iodine (V) Oxide , Part 1 : Hydration Rates. **2010**, No. V, 1–10.

(5)   Little, B. K.; Welle, E. J.; Emery, S. B.; Bogle, M. B.; Ashley, V. L.; Schrand, a M.; Lindsay, C. M. Chemical Dynamics of Nano-Aluminum/iodine (V) Oxide. *J. Phys. Conf. Ser.* **2014**, *500* (5), 052025.

(6)   Little, B. K.; Emery, S. B.; Lindsay, M. C. Physiochemical Characterization of Iodine (V) Oxide Part II Morphology and Crystal Structure of Particulat Films. *Crystals* **2015**.

(7)   Wang, H.; DeLisio, J. B.; Jian, G.; Zhou, W.; Zachariah, M. R. Electrospray Formation and Combustion Characteristics of Iodine-Containing Al/CuO Nanothermite Microparticles. *Combust. Flame* **2015**, *162* (7), 2823–2829.

(8)   Grinshpun, S. A.; Adhikari, A.; Yermakov, M.; Reponen, T.; Dreizin, E.; Schoenitz, M.; Hoffmann, V.; Zhang, S. Inactivation of Aerosolized Bacillus Atrophaeus (BG) Endospores and MS2 Viruses by Combustion of Reactive Materials. *Environ. Sci. Technol.* **2012**, *46* (13), 7334–7341.

(9)   Grinshpun, S. A.; Li, C.; Adhikari, A.; Yermakov, M.; Reponen, T.; Schoenitz, M.; Dreizin, E.; Hoffmann, V.; Trunov, M. Method for Studying Survival of Airborne Viable Microorganisms in Combustion Environments: Development and Evaluation. *Aerosol Air Qual. Res.* **2010**, *10* (5), 414–424.

(10)   Tringe, J. W.; Dugan, L. C.; Levie, H. W.; Kuhl, A. L.; Murphy, G. A.; Alves, S. W.; Vandersall, K. S.; Pantoya, M. L. Comparison of Bacillus Atrophaeus Spore Viability Following Exposure to Detonation of C4 and to Deflagration of Halogen-Containing Thermites. *J. Appl. Phys.* **2013**, *114* (23).

(11)   Zhou, Z. Q.; Nie, J. X.; Ou, Z. C.; Qin, J. F.; Jiao, Q. J. Effects of the Aluminum Content on the Shock Wave Pressure and the Acceleration Ability of RDX-Based Aluminized Explosives. *J. Appl. Phys.* **2014**, *116* (14).

(12)   Brousseau, P.; Anderson, C. J. Nanometric Aluminum in Explosives. *Propellants, Explos. Pyrotech.* **2002**, *27* (5), 300–306.

(13)   Chan, S. K. Reaction Delay of Aluminum in Condensed Explosives. *Propellants, Explos. Pyrotech.* **2014**, *39* (6), 897–903.

(14)   Julien, P.; Soo, M.; Goroshin, S.; Frost, D. L.; Bergthorson, J. M.; Glumac, N.; Zhang, F. Combustion of Aluminum Suspensions in Hydrocarbon Flame Products. *J. Propuls. Power* **2014**, *30* (4), 1047–1054.

(15)   Zheng, B.; Lin, Y.; Zhou, Y.; Lavernia, E. J. Gas Atomization of Amorphous Aluminum: Part I. Thermal Behavior Calculations. *Metall. Mater. Trans. B Process Metall. Mater. Process. Sci.* **2009**, *40* (5), 768–778.

(16)   Zheng, B.; Lin, Y.; Zhou, Y.; Lavernia, E. J. Gas Atomization of Amorphous Aluminum Powder: Part II. Experimental Investigation. *Metall. Mater. Trans. B Process Metall. Mater. Process. Sci.* **2009**, *40* (6), 995–1004.

(17)   Friedman, R.; Macek, A. Ignition and Combustion of Alumium Particles & Hot Ambient Gases. **1961**.

(18)   Osborne, D.T., Pantoya, M. L. Effect of Al Particle Size on the Thermal Degradation of Al/Teflon Mixtures. *Combust. Sci. Technol.* **2007**, *179* (8), 1467–1480.

(19)   Padhye, R., McCollum, J., Korzeniewski, C., Pantoya, M. L. Examining Hydroxyl - Alumina Bonding Toward Aluminum Nanoparticle Reactivity. *J. Phys. Chem. C* **2015**.

(20)   Kumar, R.; Saunders, R. W.; Mahajan, a. S.; Plane, J. M. C.; Murray, B. J. Physical Properties of Iodate Solutions and the Deliquescence of Crystalline I2O5 and HIO3. *Atmos. Chem. Phys.* **2010**, *10* (24), 12251–12260.

(21)   Groot, P. A. de. *Handbook of Stable Isotope Analytical Techniques*; Elsevier, 2008.

(22)   Sherwood, P. M. A. X-Ray Photoelectron Spectroscopic Studies of Some Iodine Compounds. 1976, pp 1805–1820.

(23)   Selte, K.; Kjekshus, A. Iodine Oxides Part II on the System H2O I2O5. *Acta Chem. Scand.* **1968**, *22*, 3309–3320.

(24)   Nie, H.; Schoenitz, M.; Dreizin, E. L. Calorimetric Investigation of the Aluminum –water Reaction. *Int. J. Hydrogen Energy* **2012**, *37*, 11035–11045.

(25)   Elitzur, S.; Rosenband, V.; Gany, A. Study of Hydrogen Production and Storage Based on Aluminum-Water Reaction. *Int. J. Hydrogen Energy* **2014**, *39* (12), 6328–6334.

(26)   Mahmoodi, K.; Alinejad, B. Enhancement of Hydrogen Generation Rate in Reaction of Aluminum with Water. *Int. J. Hydrogen Energy* **2010**, *35* (11), 5227–5232.

(27)   Ohmura, S.; Shimojo, F.; Kalia, R. K.; Kunaseth, M.; Nakano, A.; Vashishta, P. Reaction of Aluminum Clusters with Water. *J. Chem. Phys.* **2011**, *134*, 244702.

(28)   Lide, D. R. *CRC Handbook of Chemistry and Physics*; CRC Press, 2005.

(29)   Wikjord, A.; Taylor, P.; Torgerson, D.; Hachkowski, L. Thermal Behaviour of Corona-Precipitated Iodine Oxides. *Thermochim. Acta* **1980**, *36*, 367–375.

(30)   Skulski, L. Organic iodine(I, III, and V) Chemistry: 10 Years of Development at the Medical University of Warsaw, Poland. *Molecules* **2000**, *5* (12), 1331–1371.

(31)   Mulamba, O.; Pantoya, M. Exothermic Surface Reactions in Alumina-Aluminum Shell-Core Nanoparticles with Iodine Oxide Decomposition Fragments. *J. Nanoparticle Res.* **2014**, *16* (3).